FEBS Letters 580 (2006) 3823–3828

Induced-fitting and electrostatic potential change of PcyA upon substrate binding demonstrated by the crystal structure of the substrate-free form

Yoshinori Hagiwara[a], Masakazu Sugishima[b,1], Yasuhiro Takahashi[a], Keiichi Fukuyama[a,*]

[a] *Department of Biological Sciences, Graduate School of Science, Osaka University, 1-1 Machikaneyama-cho, Toyonaka, Osaka 560-0043, Japan*
[b] *Department of Medical Biochemistry, Kurume University School of Medicine, 67 Asahi-machi, Kurume, Fukuoka 830-0011, Japan*

Received 24 April 2006; revised 30 May 2006; accepted 30 May 2006

Available online 12 June 2006

Edited by Hans Eklund

Abstract Phycocyanobilin:ferredoxin oxidoreductase (PcyA) catalyzes the sequential reduction of the vinyl group of the D-ring and the A-ring of biliverdin IXα (BV) using ferredoxin to produce phycocyanobilin, a pigment used for light-harvesting and light-sensing in red algae and cyanobacteria. We have determined the crystal structure of the substrate-free form of PcyA from *Synechocystis* sp. PCC 6803 at 2.5 Å resolution. Structural comparison of the substrate-free form and the PcyA–BV complex shows major changes around the entrance of the BV binding pocket; upon BV binding, two α-helices and nearby side-chains move to produce tight BV binding. Unexpectedly, these movements localize the positive charges around the BV binding site, which may contribute to the proper binding of ferredoxin to PcyA. In the substrate-free form, the side-chain of Asp105 was located at a site that would be underneath the BV A-ring in the PcyA–BV complex and hydrogen-bonded with His88. We propose that BV is protonated by a mechanism involving conformational changes of these two residues before reduction.

Keywords: Redox; Induced-fit; Light-harvesting pigment; FDBR family; Phytobilin; Phycobilisome

1. Introduction

Phycobilins are members of the phytobilin chromophores, linear tetrapyrrole pigments that are used for light harvesting and/or photoreception in plants, algae, and cyanobacteria [1,2]. Phycobiliproteins, in which phycobilins are covalently bonded to the polypeptide, are assembled on the outer surface of the thylakoid membrane to form the phycobilisome, a large light-harvesting antenna complex for Photosystem II in red algae and cyanobacteria [3]. In higher plants, phytochromobilin, a phytobilin, is covalently bonded to phytochrome, a red-sensitive photoreceptor that is involved in photomorphogenesis, photoperiodic induction of flowering, chloroplast development, leaf senescence, and leaf abscission [4]. The photoisomerization of phytochromobilin is the trigger for these physiological reactions. Recently, phytochrome homologs have been found in photosynthetic and non-photosynthetic bacteria. These phytochrome homologs are covalently bonded to phycobilins or biliverdin IXα (BV), a precursor of phytobilins [2,5].

Biosynthesis of phytobilins begins with the cleavage of the porphyrin ring of heme catalyzed by heme oxygenase [6,7] to produce BV. BV is further reduced by ferredoxin-dependent bilin reductases (FDBRs) to phytobilins [1]. Because FDBRs show weak sequence homology to each other and prefer ferredoxin (Fd) as an electron donor, FDBRs have been considered to constitute a gene family [8]. Although NADPH-dependent biliverdin reductases found in mammals [9] and cyanobacteria [10] also catalyze BV reduction, these enzymes are distinct from FDBRs not only in the preference of Fd as an electron donor but also in their amino acid sequences. Phycocyanobilin:Fd oxidoreductase (PcyA), a member of the FDBR family, is unique in that it catalyzes the reduction of BV in two sequential steps to produce 3Z/3E-phycocyanobilin, one of the major pigments in the phycobilisome (Fig. 1) [11]. Upon BV binding to PcyA, neutral BV is converted into a fully N-protonated cationic form, BVH^+ [2] [12]. Then, PcyA reduces the vinyl group of the BVH^+ D-ring to generate $18^1,18^2$-dihydrobiliverdin. In the next step, PcyA reduces the A-ring of $18^1,18^2$-dihydrobiliverdin to generate 3Z/3E-phycocyanobilin. In each reduction step, two electrons are supplied by Fd. Recently, we determined the crystal structure of the PcyA–BV complex from *Synechocystis* sp. PCC 6803 at 1.51 Å resolution [13]. PcyA is folded into a three-layer α/β/α sandwich structure: four N-terminal α-helices (H1/H2/H4/H6), a seven stranded (S1–S7) antiparallel β-sheet, and five C-terminal α-helices (H3/H5/H7/H8/H9). BV has a cyclic 'porphyrin-like' conformation and is positioned between the β-sheet and C-terminal α-helices. The electrostatic potential on the molecular surface of the complex is clearly separated into acidic and basic regions, suggesting that Fd likely binds the basic patch near the BV binding pocket. Based on the structure of the BV binding pocket and the stereochemical configuration of the product, we proposed that Asp105 is critically involved in the sequential reductions by PcyA.

In this study, we have determined the crystal structure of the substrate-free form of PcyA from *Synechocystis* sp. PCC

*Corresponding author. Fax: +81 6 6850 5425.
E-mail address: fukuyama@bio.sci.osaka-u.ac.jp (K. Fukuyama).

[1] Research fellow of the Japan Society for the Promotion of Science, Japan.

Abbreviations: BV, biliverdin IXα; Fd, ferredoxin; FDBR, Fd-dependent bilin reductase; PcyA, phycocyanobilin:Fd oxidoreductase; r.m.s., root-mean-square

[2] We ignored the contribution of the propionates to the net charge on BV.

0014-5793/$32.00
doi:10.1016/j.febslet.2006.05.075

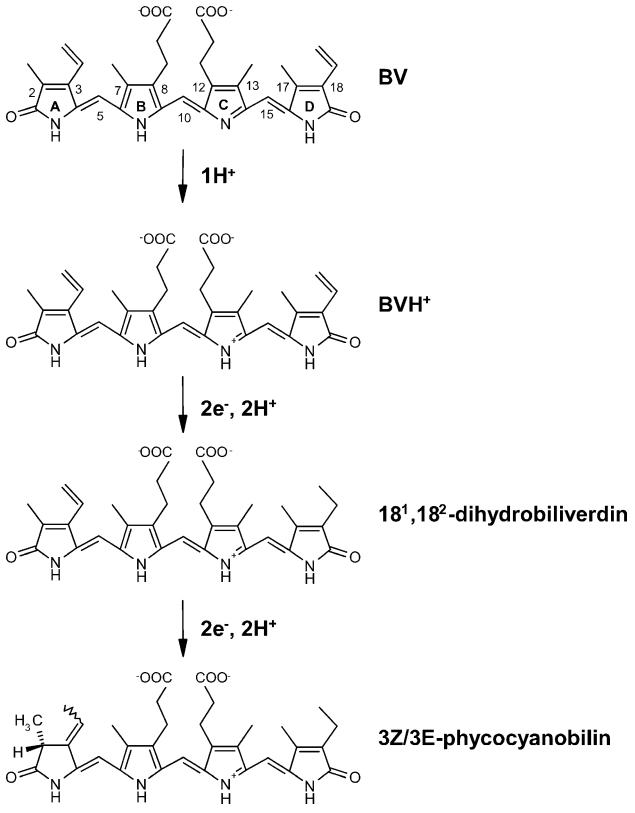

Fig. 1. Enzymatic reaction of PcyA. Upon BV binding to PcyA, it is protonated to BVH^+. BVH^+ is then reduced to 3Z/3E-phycocyanobilin via 18^1,18^2-dihydrobiliverdin using electrons supplied by ferredoxin.

6803 at 2.5 Å resolution. Structural comparison of the substrate-free form of PcyA with the PcyA–BV complex shows the interesting changes in electrostatic potential on the molecular surface; BV binding to PcyA induces the structural changes that increase the positive charges around the BV binding site. Furthermore, upon BV binding, the side-chain conformation of Asp105 markedly changes. Here, we discuss these results from the viewpoint of the characteristic PcyA reaction.

2. Materials and methods

PcyA was prepared as described [13]. Crystallization conditions for the substrate-free form of PcyA were screened by the hanging-drop vapor-diffusion method using Crystal Screen and Crystal Screen 2 kits (Hampton Research) at 293 K. PcyA (20 mg/ml) was mixed with equal volumes of each reservoir solution and equilibrated. Octahedral crystals were obtained after a few months using a reservoir solution containing 2.0 M ammonium sulfate, 0.1 M HEPES–NaOH at pH 7.5, and 2% (v/v) polyethylene glycol 400.

The crystals were soaked in crystallization solution containing 15% (v/v) glycerol as a cryo-protectant and flash-cooled under a nitrogen gas stream at 100 K. Diffraction data were collected at 100 K using synchrotron radiation ($\lambda = 1.0000$ Å) from the BL38B1 beamline at SPring-8 and a Jupiter 210 CCD detector (Rigaku). The data were processed and scaled with HKL2000 [14]. The crystal belonged to the space group $P4_32_12$ with unit-cell dimensions $a = b = 75.98$ Å and $c = 84.97$ Å. The structure of the substrate-free form was solved by the molecular replacement method using a model of the PcyA-BV complex [13] as the search probe, where BV and solvent molecules were excluded. Rotational and translational searches with MOLREP [15] in the CCP4 package [16] using the diffraction data (15.0–4.0 Å resolution) located a molecule in an asymmetric unit. The coordinates of the model and individual temperature factors were refined using CNS [17] and manually revised with Xfit [18]. After several cycles of refinement and model adjustments, water molecules and ions were included in the model. Diffraction data and refinement statistics are summarized in Table 1. Coordinates of the substrate-free form of PcyA have been deposited at the RCSB Protein Data Bank under the accession code 2DKE.

Table 1
Diffraction and refinement statistics

Diffraction statistics[a]	
Resolution (Å)	2.5
No. of observations	50826
No. of unique reflections	9064
Completeness (%)	97.6 (98.8)
Mean $I_0/\sigma(I)$	11.5 (3.6)
R_{sym}[b] (%)	7.9 (23.7)
Refinement statistics	
R[c]/R_{free}[d](%)	24.3/29.9
No. of Cl^- ion/water molecules	1/47
R.m.s. deviations from ideal values	
Bond length (Å)	0.008
Bond angle (°)	1.51
Ramachandran plot	
Most favored (%)	90.4
Additionally allowed (%)	8.7
Generously allowed (%)	1.0

[a]Values in parentheses correspond to the highest-resolution shell (2.59–2.50 Å).
[b]$R_{sym} = \sum_{hkl}\sum_i|I_i(hkl) - \langle I(hkl)\rangle|/\sum_{hkl}\sum_i I_i(hkl)$.
[c]R-factor $= \sum_{hkl}||F_o(hkl)| - |F_c(hkl)||/\sum_{hkl}|F_o(hkl)|$.
[d]R_{free} value calculated for 5% of the data set not included in refinements.

3. Results and discussion

3.1. Induced-fitting of PcyA upon BV binding

We have determined the structure of the substrate-free form of PcyA from *Synechocystis* sp. PCC 6803 at 2.5 Å resolution. The model contains 241 of the 248 residues of PcyA, together with a chloride ion and 47 water molecules. Residues 1–4 and 246–248 could not be built due to poor electron density. The overall structure of the substrate-free form was similar to that of the complex [13] (root-mean-square [r.m.s.] distance between the corresponding Cαs was 1.19 Å for 240 residues), but notable structural differences were observed in the A-loop, H2′, the B-loop, S4, H5, and H8 (Fig. 2a and supplementary Fig. 1a). In the substrate-free form, the α-helical structures from Leu13 to Pro15 (H1) and from Pro153 to Ile157 (H5) were disrupted, and a new α-helical structure was formed between Glu44 and Gly47 (H2′). H5 and H8, which constitute the entrance of the substrate binding pocket, moved so that the entrance was narrowed upon BV binding (Fig. 2b). This movement increases the hydrophobic interaction between PcyA and the BV tetrapyrrole ring to stabilize the PcyA–BV complex. In addition, several hydrophilic interactions formed upon the conformational changes associated with BV binding. Trp154 in H5 and Lys221 in H8 formed a hydrogen-bond and a salt-bridge, respectively, to the propionate groups of BV when these helices moved upon BV binding. Moreover, the

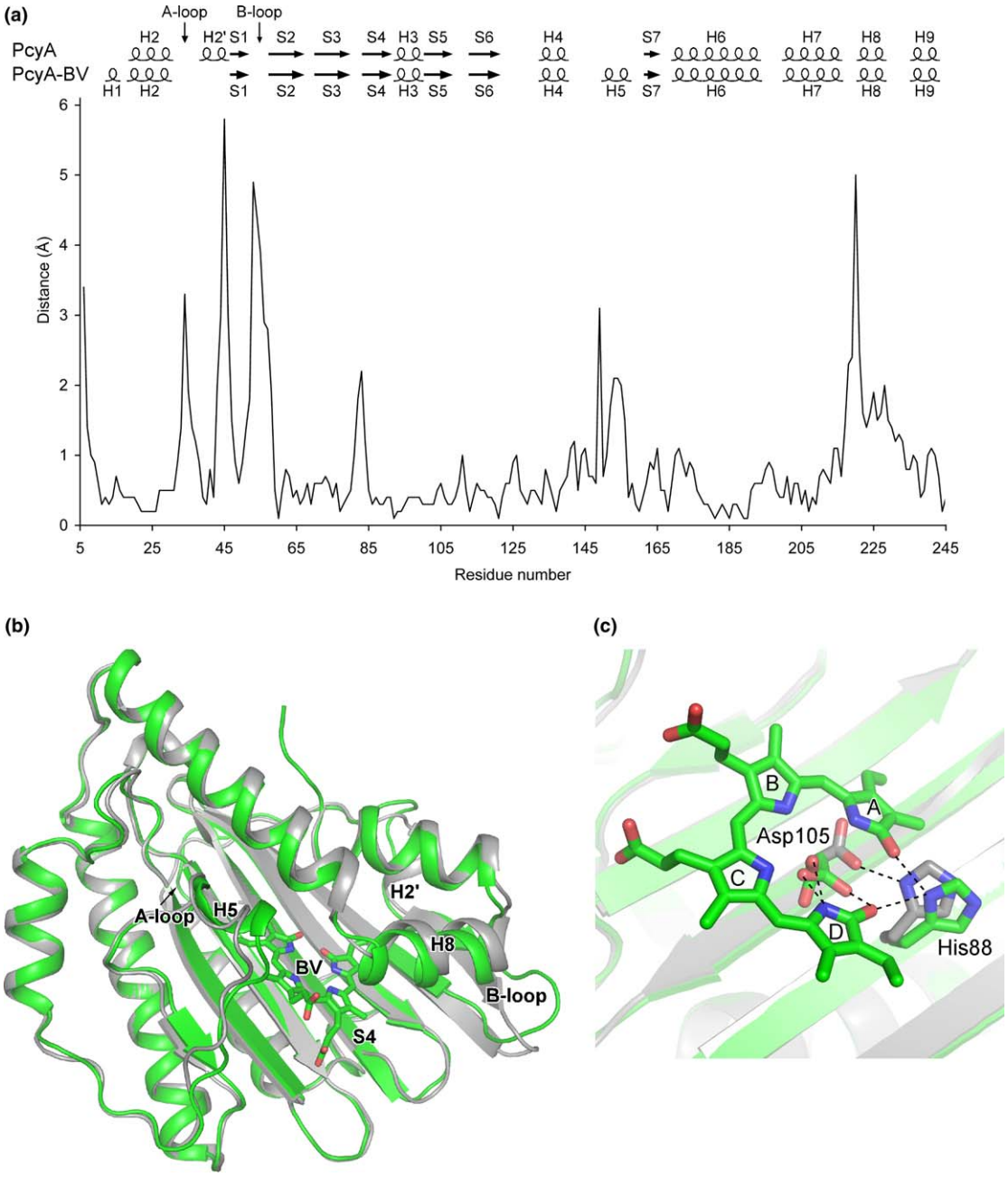

Fig. 2. Structural changes upon BV binding. The substrate-free form of PcyA was superimposed on the PcyA–BV complex so as to minimize the r.m.s. distances between corresponding Cαs. (a) Distances between corresponding Cα pairs of Leu6-Asp245 are plotted. The secondary structures of the substrate-free form and the complex are shown above the plot. (b) Superposition of ribbon drawings (gray; the substrate-free form, green; the complex). BV is shown using the stick model, in which red and blue show oxygen and nitrogen atoms, respectively. The figure was prepared with PyMOL [23]. (c) Close-up view of the BV binding pocket. The colors of the substrate-free form and complex are the same as shown in b. Dashed lines indicate hydrogen-bonds. Asp105 in the complex took on two conformations; in the major conformation, the side-chain formed hydrogen-bonds with both the lactam oxygen and nitrogen atoms of the D-ring, while it only formed a hydrogen-bond with the lactam nitrogen atom in the minor conformation. In the substrate-free form, the side-chain of Asp105 was located at a site that would be underneath the BV A-ring in the complex, and formed a hydrogen-bond with His88.

side-chain conformation of Trp154 changed to optimize the formation of a hydrogen-bond with the propionate group through a water molecule. The side-chain of Arg149, adjacent to H5, was disordered in the substrate-free form, whereas it formed a salt-bridge to the propionate group of BV in the complex.

Notably, the hydrogen-bonding of His88 and Asp105, candidate catalytic residues [13], changed upon BV binding. His88 hydrogen-bonded with the lactam oxygen atoms of the A-ring and D-ring in the complex, whereas it hydrogen-bonded with Asp105 in the substrate-free form (Fig. 2c and supplementary Fig. 1b). Structural changes of Glu76, Tyr212

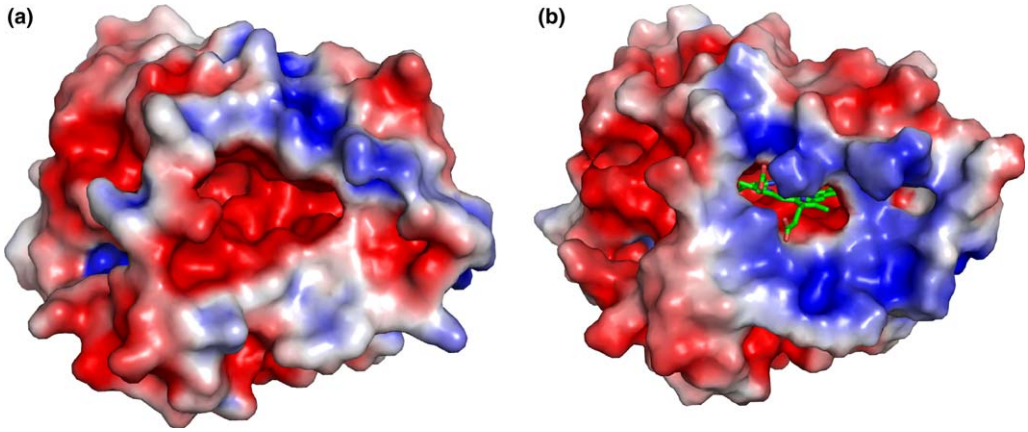

Fig. 3. Electrostatic potentials of the substrate-free and complexed forms. Positive and negative surfaces are shown in blue and red, respectively ((a) substrate-free form, (b) complexed form, ±3 kT/e). Electrostatic potential was calculated with PyMOL and APBS [24], where solvent dielectric contribution (the dielectric constant of the solvent was 80 and that of the protein was 2) was taken into account.

and Gln216, which are also involved in the catalytic reaction, were less significant than those of His88 and Asp105. Comparison of the temperature factors of the substrate-free form and the complex shows that the average temperature factor of Gln216 (62.0) is higher than that of all residues (46.5) in substrate-free form whereas that of Gln216 (14.8) is lower than that of all residues (18.7) in the complex. Gln216 appears to be more mobile in the substrate-free form than in the complex. The high mobility in the substrate-free form may be due to the absence of hydrogen-bonds with Tyr212 and with BV through a water molecule that were present in the complex.

3.2. Electrostatic potential change upon BV binding

In the complex, positively charged surface areas are clearly localized around the BV binding site; this localization most likely serves to properly bind Fd, an acidic electron-transfer protein, to the BV binding site [13,19,20]. We noted interesting differences in the electrostatic potential of the molecular surfaces of the substrate-free form and the complex (Fig. 3); in the substrate-free form, the positive charges are dispersed. The observed differences in electrostatic potential are caused by small structural changes upon BV binding. First, helix H5 (Pro153–Ile157), which forms upon BV binding and is known to have a dipole, directs its positively charged N-terminus toward the binding pocket [21]. In addition, approach of the N-terminal region of H8 (Fig. 2b) increases the positive charge near the entrance of the BV binding site. Second, the disordered side-chain of Arg149 in the substrate-free form forms a salt-bridge with the propionate group of BV in the complex. Third, the carboxyl groups of Glu54 and Glu150, which are positioned toward the BV binding site in the substrate-free form, are positioned outside the BV binding site in the complex. Formation of helix H5 and the rearrangements of basic and acidic residues upon BV binding enhance the localization of positive charges around the BV binding site, which may increase the efficiency of proper recognition of the PcyA surface by the negatively charged Fd.

3.3. Protonation scheme of the pyrrole ring of BV

Spectroscopic analysis of the PcyA–BV complex has indicated that the neutral BV molecule is protonated to BVH^+ upon binding to PcyA prior to reduction by Fd (Fig. 1) [12]. The resonance structures of BVH^+ suggest that the positive charge is spread over the tetrapyrrole ring. The formation of the cationic species of BV in the complex would facilitate electron transfer from Fd. A previous report that Asp105 in the complex forms hydrogen-bonds to the lactam nitrogen atoms of BV [13] suggests that Asp105 is the primary candidate for direct protonation of BV upon binding. The carboxyl group of Asp105 should be protonated again in the complex, as judged by the hydrogen-bonding scheme to the BV D-ring. This study has demonstrated that the side-chain of Asp105 changes the conformation upon BV binding: in the substrate-free form, the side-chain of Asp105 was located at a site that would be underneath the BV A-ring in the complex and hydrogen-bonded with His88 (Fig. 2c). In the complex, the conserved His88, His74, and Asn62 residues form a hydrogen-bond network via a water molecule from the BV binding site to the molecular surface. Although the presence of the water molecule connecting His74–Asn62 was unclear in the substrate-free form due to limited resolution, this network should be conserved in the substrate-free form and provide protons to Asp105 for protonation/de-protonation of the carboxyl group.

On the basis of these findings, we propose a mechanism for the protonation of BV to BVH^+ upon BV binding as shown in Fig. 4. First, the Nδ of His88 protonates the carboxyl group of Asp105 upon BV binding, then Asp105 undergoes a conformational change and transfers a proton to BV. Next, His88 is protonated by the hydrogen-bond network and Asp105 changes conformation to form a hydrogen-bond with His88. Finally, Asp105 is re-protonated by His88 and changes conformation to form a hydrogen-bond with the BV D-ring. Recent mutagenetic analysis of PcyA of *Nostoc* sp. PCC 7120 shows that H85Q and D102N mutants, which correspond to H88Q and D105N in *Synechocystis* PcyA, can bind BV. However, the spectra of these BV complexes do not have a shoulder in the far-red region above 700 nm [22], indicating that these mutants cannot protonate BV upon binding. This result supports the proposed mechanism that BV is protonated through His88 and Asp105 before reduction.

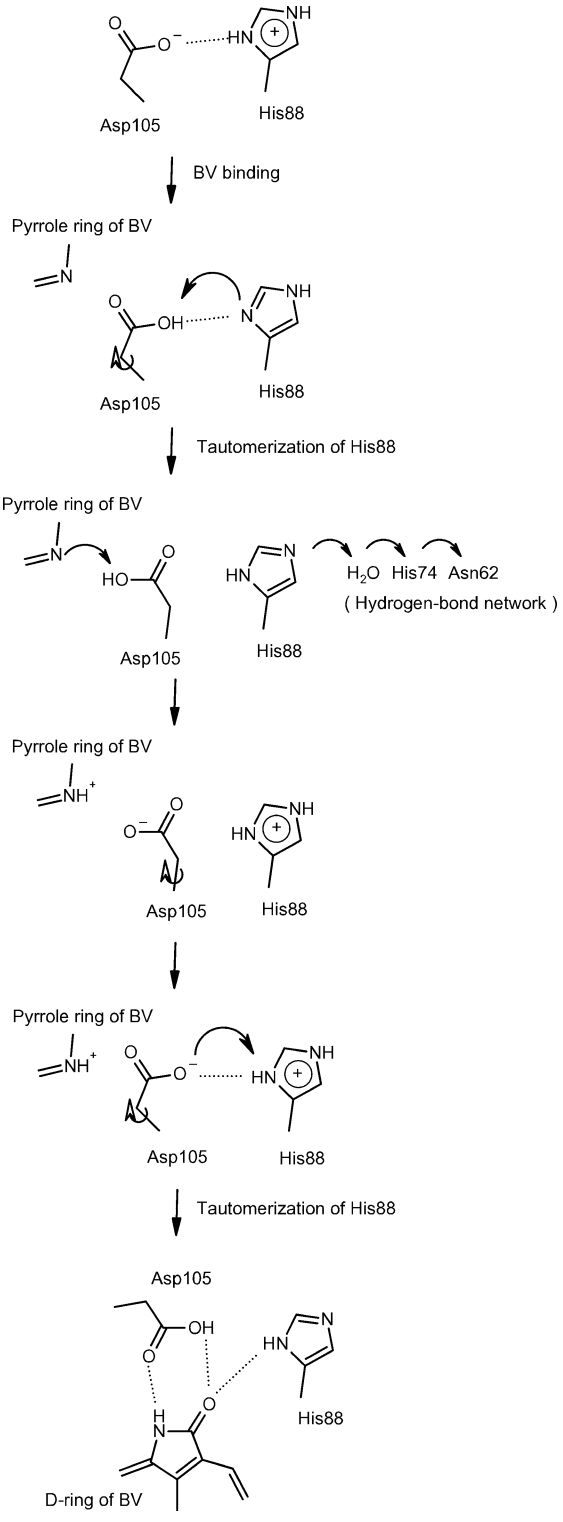

Fig. 4. Proposed mechanism of the protonation of BV to BVH^+.

Acknowledgments: We thank Drs. Hisanobu Sakai and Kazuya Hasegawa (Japan Synchrotron Radiation Research Institute) for their aid with data collection using the synchrotron radiation at SPring-8 (Proposal number 2005A0214-NL1-np), and Prof. Masato Noguchi (Kurume University School of Medicine) for advice and encouragement. This work was supported in part by Grants-in-Aid for Scientific Research (Grants 16570095 and 17053014 to K.F.), by a grant-in-aid for Research Fellows of the Japan Society for the Promotion of Science (Grant 17.5063 to M.S.), and by a grant of the National Project on Protein Structural and Functional Analyses from the Ministry of Education, Culture, Sports, Science, and Technology of Japan.

Appendix A. Supplementary data

Supplementary data associated with this article can be found, in the online version, at doi:10.1016/j.febslet.2006.05.075.

References

[1] Beale, S.I. (1993) Biosynthesis of phycobilins. Chem. Rev. 93, 785–802.
[2] Hughes, J. and Lamparter, T. (1999) Prokaryotes and phytochrome. The connection to chromophores and signaling. Plant. Physiol. 121, 1059–1068.
[3] Grossman, A.R., Schaefer, M.R., Chiang, G.G. and Collier, J.L. (1993) The phycobilisome, a light-harvesting complex responsive to environmental conditions. Microbiol. Rev. 57, 725–749.
[4] Schafer, E. and Bowle, C. (2002) Phytochrome-mediated photoperception and signal transduction in higher plants. EMBO Rep. 3, 1042–1048.
[5] Wagner, J.R., Brunzelle, J.S., Forest, K.T. and Vierstra, R.D. (2005) A light-sensing knot revealed by the structure of the chromophore-binding domain of phytochrome. Nature 438, 325–331.
[6] Migita, C.T., Zhang, X. and Yoshida, T. (2003) Expression and characterization of cyanobacterial heme oxygenase, a key enzyme in the phycobilin synthesis. Properties of the heme complex of recombinant active enzyme. Eur. J. Biochem. 270, 687–698.
[7] Cornejo, J., Willows, R.D. and Beale, S.I. (1998) Phytobilin biosynthesis: cloning and expression of a gene encoding soluble ferredoxin-dependent heme oxygenase from *Synechocystis* sp. PCC 6803. Plant J. 15, 99–107.
[8] Frankenberg, N., Mukougawa, K., Kohchi, T. and Lagarias, J.C. (2001) Functional genomic analysis of the HY2 family of ferredoxin-dependent bilin reductases from oxygenic photosynthetic organisms. Plant Cell 13, 965–978.
[9] Noguchi, M., Yoshida, T. and Kikuchi, G. (1979) Purification and properties of biliverdin reductases from pig spleen and rat liver. J. Biochem. (Tokyo) 86, 833–848.
[10] Schluchter, W.M. and Glazer, A.N. (1997) Characterization of cyanobacterial biliverdin reductase. Conversion of biliverdin to bilirubin is important for normal phycobiliprotein biosynthesis. J. Biol. Chem. 272, 13562–13569.
[11] Frankenberg, N. and Lagarias, J.C. (2003) Phycocyanobilin:ferredoxin oxidoreductase of *Anabaena* sp. PCC 7120. Biochemical and spectroscopic characterization. J. Biol. Chem. 278, 9219–9226.
[12] Tu, S.L., Gunn, A., Toney, M.D., Britt, R.D. and Lagarias, J.C. (2004) Biliverdin reduction by cyanobacterial phycocyanobilin:ferredoxin oxidoreductase (PcyA) proceeds via linear tetrapyrrole radical intermediates. J. Am. Chem. Soc. 126, 8682–8693.
[13] Hagiwara, Y., Sugishima, M., Takahashi, Y. and Fukuyama, K. (2006) Crystal structure of phycocyanobilin:ferredoxin oxidoreductase in complex with biliverdin IXα, a key enzyme in the biosynthesis of phycocyanobilin. Proc. Natl. Acad. Sci. USA 103, 27–32.
[14] Otwinowski, Z. and Minor, W. (1997) Processing of X-ray diffraction data collected in oscillation mode. Methods Enzymol. 276, 307–326.
[15] Vagin, A. and Teplyakov, A. (1997) MOLREP: an automated program for molecular replacement. J. Appl. Cryst. 30, 1022–1025.

[16] Collaborative Computational Project Number 4 (1994) The CCP4 suite: programs for protein crystallography. Acta Crystallogr. D 50, 760–763.
[17] Brünger, A.T. et al. (1998) Crystallography & NMR system: a new software suite for macromolecular structure determination. Acta Crystallogr. D 54, 905–921.
[18] McRee, D.E. (1999) XtalView/Xfit – a versatile program for manipulating atomic coordinates and electron density. J. Struct. Biol. 125, 156–165.
[19] van den Heuvel, R.H., Svergun, D.I., Petoukhov, M.V., Coda, A., Curti, B., Ravasio, S., Vanoni, M.A. and Mattevi, A. (2003) The active conformation of glutamate synthase and its binding to ferredoxin. J. Mol. Biol. 330, 113–128.
[20] Fukuyama, K. (2004) Structure and function of plant-type ferredoxins. Photosynth. Res. 81, 289–301.
[21] Wada, A. (1976) The alpha-helix as an electric macro-dipole. Adv. Biophys. 9, 1–63.
[22] Tu, S.L., Sughrue, W., Britt, R.D. and Lagarias, J.C. (2006) A conserved histidine–aspartate pair is required for exovinyl reduction of biliverdin by a cyanobacterial phycocyanobilin:ferredoxin oxidoreductase. J. Biol. Chem. 281, 3127–3136.
[23] DeLano, W.L. (2002) The PyMOL Molecular Graphics System, DeLano Scientific, San Carlos, CA, USA.
[24] Baker, N.A., Sept, D., Joseph, S., Holst, M.J. and McCammon, J.A. (2001) Electrostatics of nanosystems: application to microtubules and the ribosome. Proc. Natl. Acad. Sci. USA 98, 10037–10041.